Copper-Rich Planar Defects in Gd-Substituted Superconductors

H. SHIBAHARA* AND L. D. MARKS

Department of Material Science and Engineering and Materials Research Center, Northwestern University, Evanston, Illinois 60208

AND S.-J. HWU† AND K. R. POEPPELMEIER

Department of Chemistry and Materials Research Center, Northwestern University, Evanston Illinois 60208

The structure of the high-temperature superconductor $GdBa_2Cu_3O_x$ ($x \approx 7$) was examined by high-resolution transmission electron microscopy. The Gd-substituted superconductors, in contrast to the yttrium-based materials, contained a large number of planar defects corresponding to a shear vector of 1/6 [301]. Detailed image simulation enabled the defects to be identified as copper-rich regions. © 1989 Academic Press, Inc.

Introduction

Following the discovery of superconductivity in the temperature range 30–40 K for the La–Ba–Cu–O system (*1*), extensive interest focused on the Y–Ba–Cu–O system where it was found that $YBa_2Cu_3O_7$ exhibits a remarkably high T_c above liquid nitrogen temperature (*2*). Subsequently, it was shown that when yttrium (Y) is replaced by the rare-earth elements La, Nd, Sm, Eu, Gd, etc., comparable transition temperatures could be obtained (*3–16*).

To explain the physical source of the superconductivity, it is essential to determine the crystal structure. X-ray and neutron dif-

fraction data have shown that the basic structure of $YBa_2Cu_3O_x$ ($x \approx 7$) is an oxygen-deficient perovskite structure (*17–20*). But, to obtain a detailed understanding of the relationship between the superconducting properties and the crystal structure, the local structure on a microscopical level, which cannot be determined by X-ray or neutron diffraction, must also be elucidated. High-resolution electron microscopy is a powerful method of investigating the local structure in real and reciprocal space simultaneously and the occurrence of, for instance, twinning, amorphous phases, planar defects, and oxygen defect ordering (*21–34*). In order to study the relationship between the defects in the specimen and the superconductive properties, it is important to pay special attention to the origin of the defects. That is, it is necessary to check whether the defects are consequences of

* On leave from Department of Chemistry, Kyoto University of Education, Fushimiku, Kyoto 612, Japan.
† Present address: Department of Chemistry, Rice University, Houston, TX 77251.

194

mechanical deformation during sample preparation or damage during beam irradiation. In either case it would be incorrect to view them as intrinsic defects in relation to the superconducting properties. Many electron microscopy observations of defects have been due to mechanical deformation, which characteristically exhibits a high local density.

On the basis of high-resolution electron microscope analysis, we report here the presence of defects in $GdBa_2Cu_3O_x$ ($x \approx 7$) consisting of Cu-rich planes. In our observations, the defects contained in the specimen were found to be distributed widely and uniformly throughout the specimen.

Experimental Method

Specimens of $GdBa_2Cu_3O_x$ ($x \approx 7$) were prepared by the solid-state reaction of gadolinium oxide (99.999%), barium carbonate (99.999%), and cupric oxide (99.999%). Powders were ground and calcined in air at 900°C for 2 weeks with repeated grindings. The compound was finally reheated in an oxygen atmosphere for 12 hr at 900°C and then 8 hr at 550°C. X-ray diffraction patterns of the final polycrystalline materials were taken on a Rigaku diffractometer using $CuK\alpha$ radiation and a Ni filter. An internal NBS Si standard was recorded with the sample. The lattice parameters were then refined by a least-squares method. Specimens for the electron microscope were crushed with care to limit mechanical deformation and mounted on holey carbon films without suspension to avoid degradation by water or other solvents. High-resolution observations were carried out at room temperature in an H-9000 electron microscope with a top entry goniometer stage. In order to detect the difference in structure due to the stacking sequence brought about by the irregular cation composition, a very thin fragment was selected and its orientation was adjusted until the incident beam direction was normal to the c^*-axis in reciprocal space. Image simulations based on the multislice method were carried out on an Apollo 660 workstation ring using the NUMIS programs written at Northwestern University.

Results

The sample used for observation gave an X-ray powder diffraction pattern that was quite similar to that of $YBa_2Cu_3O_x$ ($x \approx 7$). The powder sample proved to be orthorhombic with unit cell parameters $a = 0.384$, $b = 0.390$, and $c = 1.171$ nm. The very small difference in the lattice parameters from that of $YBa_2Cu_3O_x$ ($x \approx 7$) is presumably due to the slight difference in ionic radii of Gd and Y. The resistance of a Gd $Ba_2Cu_3O_x$ ($x \approx 7$) specimen as a function of temperature was measured and the critical temperature T_c, defined as the midpoint of 10 and 90% of the transition, was 93.6 K with a width of 2.8 K. The defect free structure, which is similar to that determined by neutron and X-ray diffraction (13–15) for $YBa_2Cu_3O_x$ ($x \approx 7$), is shown schematically in Fig. 3d.

Figure 1a shows experimental images obtained with the beam along the [100] or [010] direction. (The small difference between [100] and [010] is not differentiated here.) Inset in Fig. 1a is a calculated image for the following imaging condition, a sample thickness of 3.8 nm, defocus −30 nm, Cs = 0.9 mm, an accelerating voltage of 300 kV, a focal spread of 80 nm, and a convergence of 1.0 mrad. The framework of 1 unit cell is indicated in Fig. 1a. The experimental image shows the ideal structure of $GdBa_2Cu_3O_x$ ($x \approx 7$) without any defects. Figure 1b shows a high-resolution image without any defects taken along the [110] direction together with a calculated image for a thickness of 3.8 and −25 nm defocus. The framework shown indicates the unit cell size projected along the [110] direction.
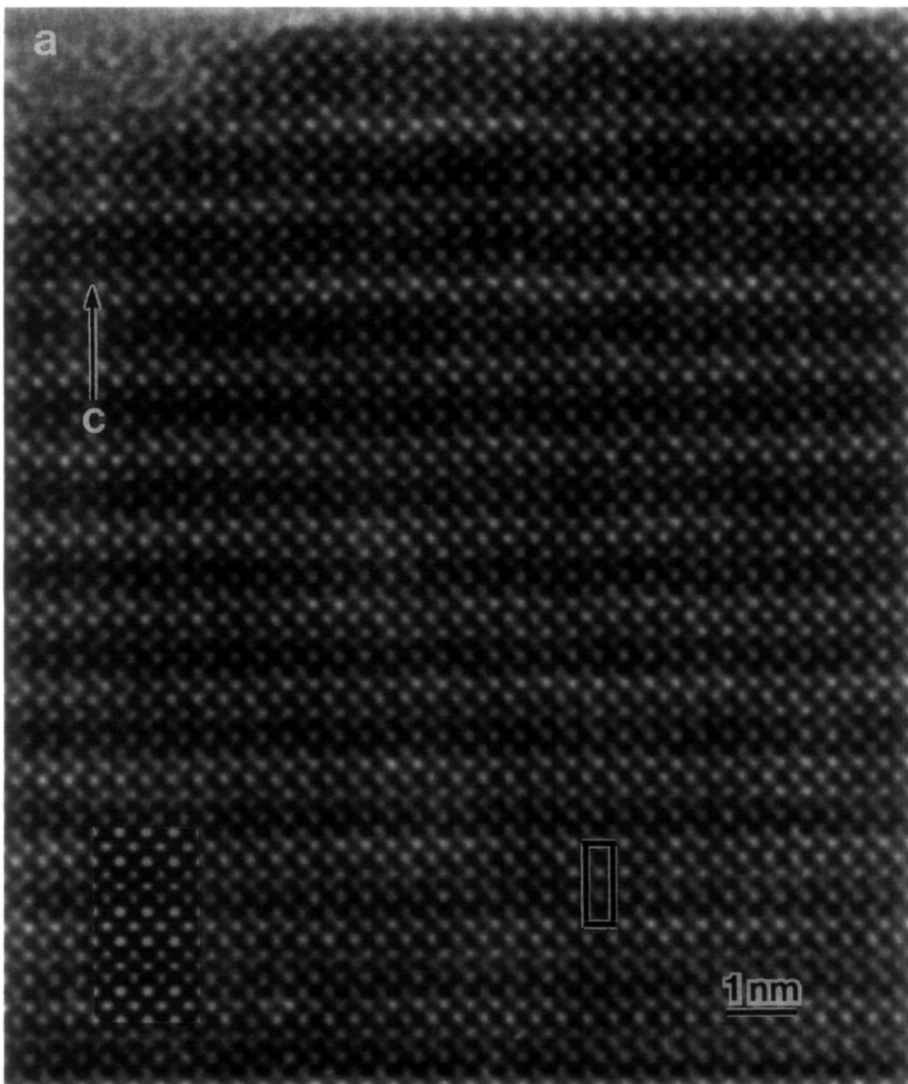
FIG. 1. (a) High-resolution electron micrograph of GdBa$_2$Cu$_3$O$_x$ ($x \approx 7$) without any defects with the incidence beam normal to the c-axis; inset is a calculated image for a thickness of 3.8 nm and a defocus of -30 nm. (b) High-resolution electron micrograph for the [110] direction, showing a perfect region; inset is a calculated image for the same conditions as in (a). The frameworks shown in (a) and (b) indicate the projected unit cell.

For the imaging conditions of Figs. 1a and 1b, the calculated images agree with the experiment, leading to the conclusion that the black dots show the positions of the metal atoms such as Gd, Ba, and Cu.

Figure 2 is an example of a high-resolu-tion image showing the typical image contrast of the planar defects. The sample was not subjected to change in structure by electron beam irradiation during observation. At least two kinds of image contrast due to defects in the specimen can be ob-
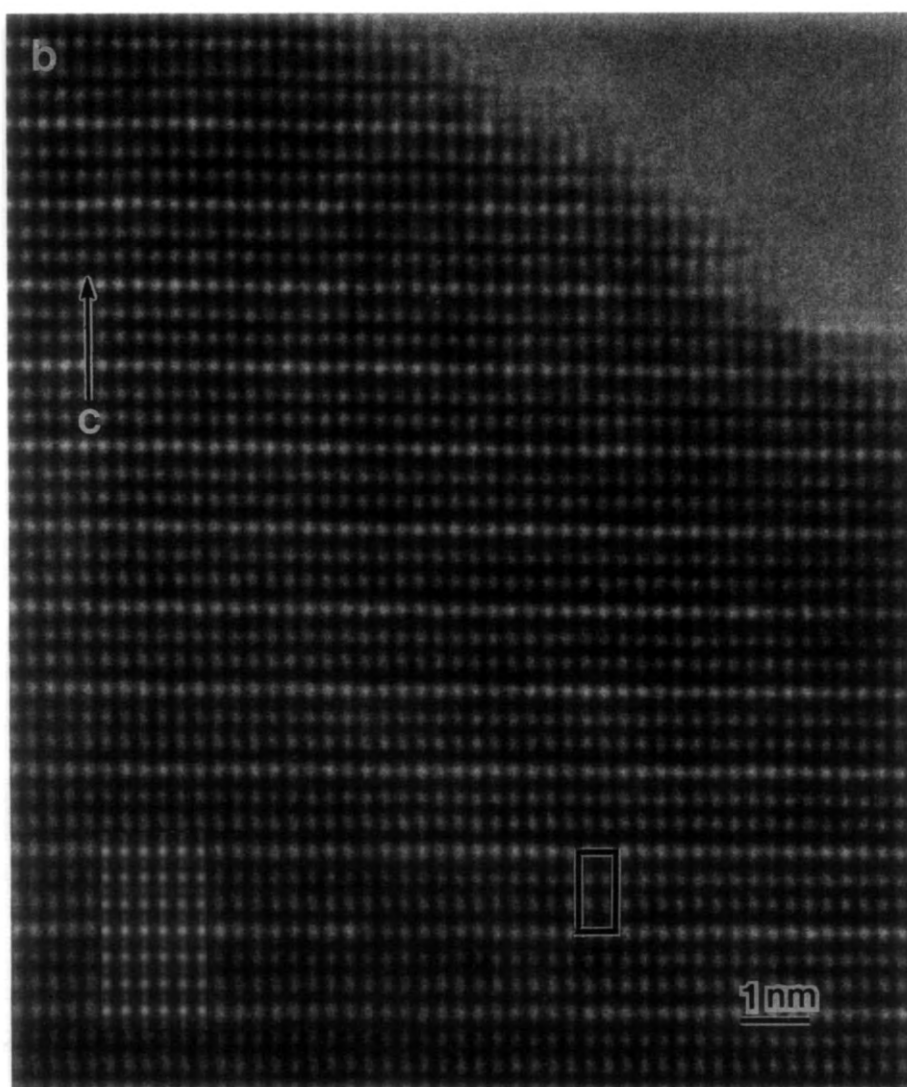
FIG. 1.—*Continued*

served as indicated by the marks S_1 and S_2 in Fig. 2. In the region S_1 the image shows a shear structure normal to the c-axis. On the other hand, S_2 shows an anomalous row of white spots between two layers as indicated by the arrow. In this region a shear structure could not be observed, but the distance between two layers is larger than that of the nominal structure. Both can be interpreted by assuming that an extra cation (Cu) layer has been introduced between two layers.

In order to discuss the structure of the defects corresponding to those shown in Fig. 2, three possible structural models are illustrated schematically in Figs. 3a–3c, with the ideal structure (*17*) shown in Fig. 3d for reference. The structures in Fig. 3 all have a shear with a displacement vector of
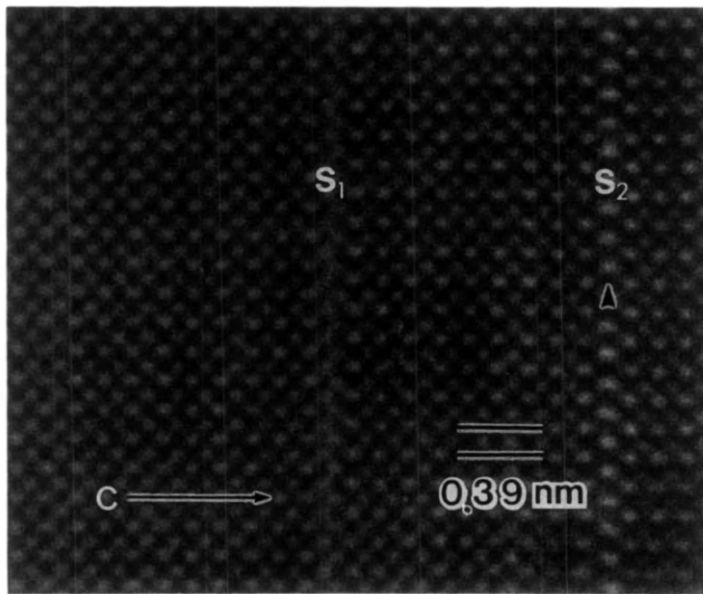
FIG. 2. High-resolution image showing two kinds of planar defects in $GdBa_2Cu_3O_x$ ($x \approx 7$).

1/6[301], with reference to the ideal struc-
ture, and were derived by taking the repul-
sion between the neighboring ions into con-
sideration. The arrows in Figs. 3a–3c
indicate the positions of the extra layers
containing copper and oxygen atoms be-
tween Ba–Ba, Gd–Gd, and Ba–Gd atoms,
respectively. In Fig. 3, although the posi-
tions of oxygen atoms are omitted, they are
considered in the calculation based on the
ideal structure (17). Namely, the copper at-
oms in each double layer are assumed to be
surrounded by a square of oxygen in the b–
c plane. Unfortunately the images are not
sufficiently sensitive to oxygen to confirm
the existence of all four of these oxygen
atoms, or whether any additional oxygen is
present on the vacant oxygen sites along
the a-axis. The imaging conditions for the
calculations were determined by consider-
ing the image contrast of the perfect struc-
ture.

An experimental through-focal series of
images showing the same defect as that at
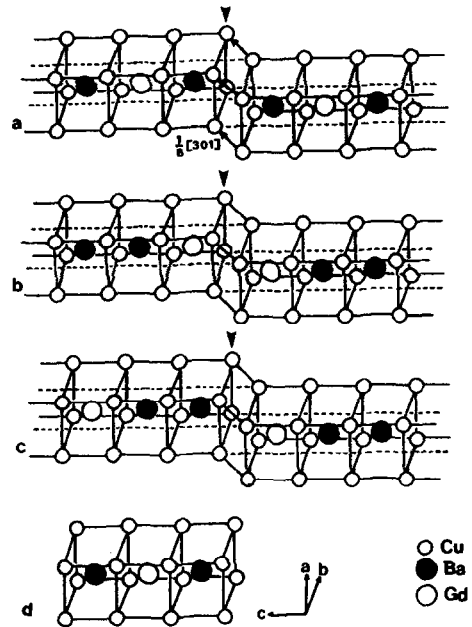the S_1 region in Fig. 2 is shown in Fig. 4.

FIG. 3. Some possible structure models containing
defects with a shear vector of 1/6 [301]. The arrows
indicate the Cu-rich regions. The Cu-rich regions are
located between (a) Ba–Ba atoms, (b) Gd–Gd atoms,
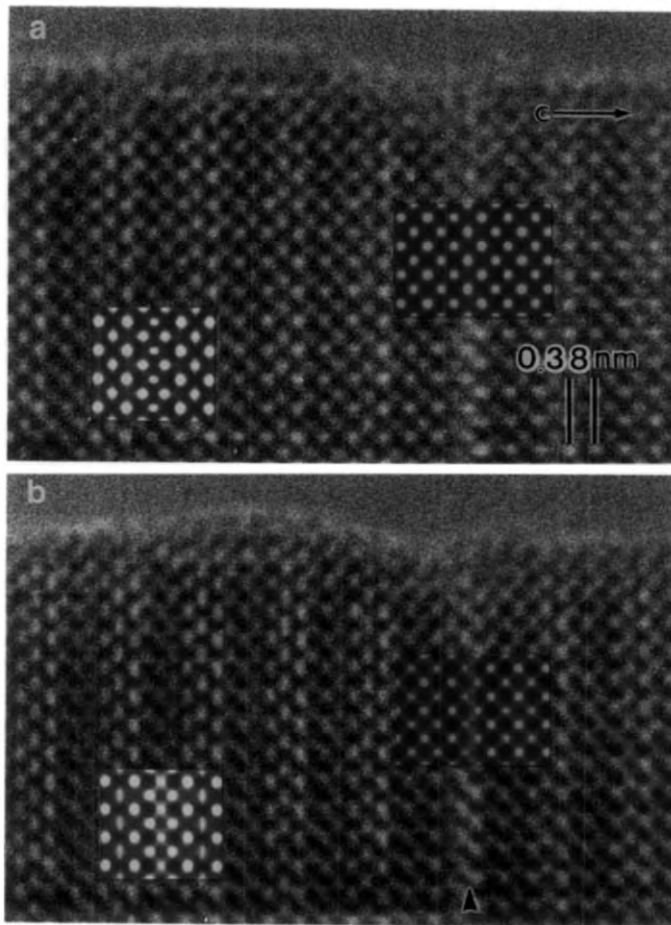(c) Ba–Gd atoms. (d) The perfect structure.

FIG. 4. Observed and calculated images of the defect along the [010] direction; the thickness is 3.4 nm and the defocus values are −70 and −60 nm.

Corresponding calculated images using the structure model of Fig. 3a for imaging conditions of a thickness of 3.4 nm, and defocus values of −70 and −60 nm are shown in the insets of Figs. 4a and 4b. According to the notation of Fig. 3a, the incident beam in the calculation is along [010]. Calculated images of the ideal structure for reference are also inset. As indicated by an arrow in Fig. 4b, a shift of half of the spacing of (100) lattice planes was observed in the images. The observed images in Fig. 4 are in reasonably good agreement with the calculated

images in the insets. It was also found from the results of the simulations that the defect structures for a thickness of less than 3 nm were not readily observable.

For further analysis of the defects observed in the region S_2 in Fig. 2, image calculations with the incidence beam along the [100] direction were performed and compared to experimental images. The region marked R in Fig. 5b shows the contrast of a perfect structure with a regular stacking. The anomalous image contrast showing the white spots is found in region D of Fig. 5b.
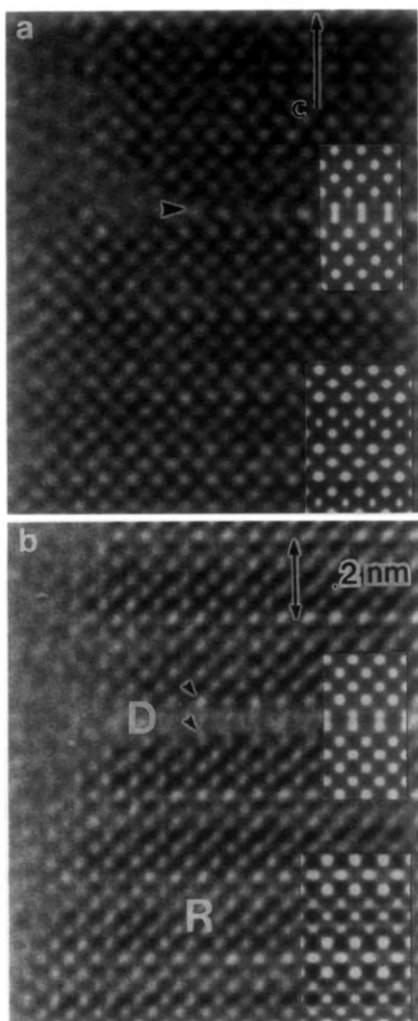
FIG. 5. Observed and calculated images of the defects along a [100] direction; the thickness is about 4.0 nm and the defocus values are −75 and −25 nm. Region D in (b) shows the pairs of Cu atoms between Ba–Gd atoms.

In region D the distance between two layers is separated by about 0.65 nm which is about 1.7 times the normal distance associated with elongated spots along the c-axis. It should be noticed that the white spots indicated by the arrows show asymmetrical contrast in Fig. 5b. In order to explain this

feature, results of calculated images based on the structure models shown in Figs. 3a–3c were compared as shown in Figs. 6a–6c. Figures 6a, 6b, and 6c were obtained by assuming that there exist Cu-rich regions between Ba–Ba, Gd–Gd, and Ba–Gd atoms, respectively, which correspond to the structure models of Fig. 3a, 3b, and 3c, respectively. Calculations were performed for a thickness of 3.2 nm and defocus values of −75, −65, −35, and −25 nm. The arrows e in Fig. 6 indicate the copper-rich regions. The white spots represent the atomic positions of cations such as Ba, Gd, Cu for the defoci of −75 and −65 nm, and the image contrast reverses for −35 and −25 defoci. While in Figs. 6a and 6b the images are symetrical, asymetrical white spots appeared in the case of the −35 and −25 nm defoci of Fig. 6c as indicated by arrows. It is difficult to distinguish between Figs. 6a, 6b, and 6c just from the image contrast; however, by comparison with the perfect crystal regions adjacent to the defects, it is clear that in this case the best agreement with Fig. 5 is Fig. 6c. Calculated images corresponding to the structure of the defect in Fig. 3c with the defocus values of −75 and −25 nm in underfocus are shown in the insets of Figs. 5a and 5b, respectively. The sample thickness was estimated to be about 4.0 nm. From the image simulations, the regions that include the planar defects with elongated white spots along the c-axis in this case can be identified as copper-rich pairs of Cu planes between Ba–Gd atoms. (It should be noted that the other defects observed contained the additional copper in the basal plane between two Ba atoms.)

Observations with the incidence parallel to the [110] direction are required to confirm the proposed structures. Figs. 7a, 7b, and 7c are through-focus images with the corresponding calculated results (using the structure model of Fig. 3a) inset, showing
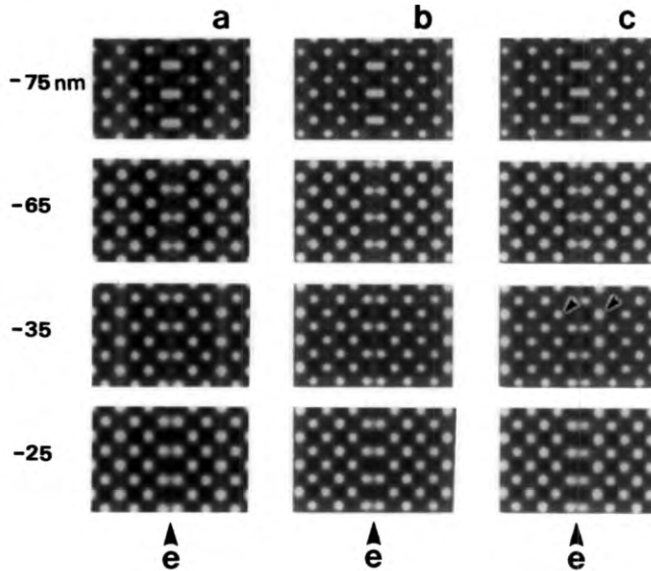
FIG. 6. A series of the calculated images using the structure models in Figs. 3a–3c. Note the asymmetrical white spots as indicated by arrows in (c).

defects identified with that of Fig. 4 as indicated by an arrow in Fig. 7a. From the image contrast the thickness of the specimen was estimated to be about 3.1 nm and the defocus values −75, −35, and −25 nm. Calculated images of the defects and nominal perfect structure shown in the insets are in good agreement with the observed images. the images along the [110] direction demonstrate the presence of a shift of half of a lattice spacing along [110] direction as expected for the proposed structure model of Fig. 3a.

Discussion

On the basis of the high-resolution electron microscopy observations, the structural defects in $GdBa_2Cu_3O_x$ ($x \approx 7$) shown in Figs. 3a and 3c were confirmed. With these two models, the image contrast indicated by S_1 and S_2 in Fig. 2 can be interpreted as an additional copper plane with a shift of 1/6 [301] or 1/6 [031], respectively. The most common observation was of an additional Cu in the basal plane between the two Ba atoms, although we have also detected the presence of the defect plane between Gd and Ba. A question is the origin of defects found in the present sample. To understand this, it should be mentioned that one can prepare copper-rich yttrium superconductors by quenching from 950°C and then reannealing (35). These results indicate that copper can be metastably retained within the superconductors. We suspect that this may also be the case for the gadolinium materials. At higher levels of copper retention, one can generate metastable copper and other rare-earth-containing rich phases by oxidation of metallic precursors such as $Yb_2Ba_4Cu_7O_x$ (36) or $Yb_2Ba_4Cu_8O_x$ (37, 38), or by laser evaporation on $SrTiO_3$ (39). Their effect on the superconducting properties is an important question to pursue.
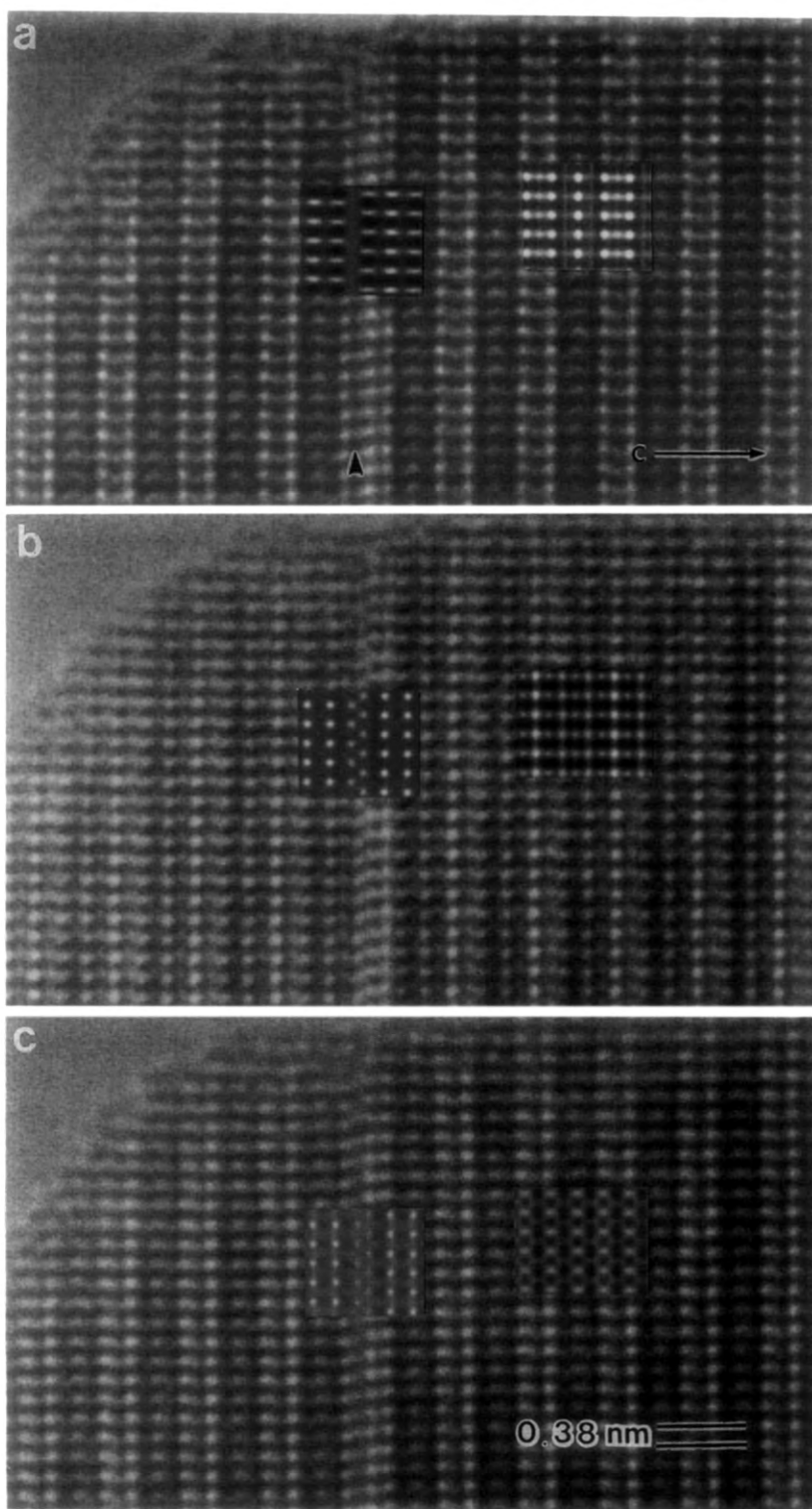
FIG. 7. Observed and calculated images of a defect along the [110] direction; the thickness is about 3.1 nm and the defocus values are −75, −35, and −25 nm.

Acknowledgments

References

1. J. G. BEDNORZ AND K. A. MULLER, *Z. Phys.* **64**, 189 (1986).
2. M. K. WU, J. R. ASHBURN, C. J. TORNG, P. H. HOR, R. L. MENG, L. GAO, Z. J. HUNG, Y. Q. WANG, AND C. W. CHU, *Phys. Rev. Lett.* **58**, 908 (1987).
3. H. W. ZANDBERGEN, G. F. HOLLAND, P. TEJEDOR, R. GRONSKY, AND A. M. STACY, *Adv. Ceram. Mater.* **2**(3B), 688 (1987).
4. C. JIANG, YU MEI, S. M. GREEN, H. L. LUO, AND C. POLITIS, *Z. Phys.* **68**, 15 (1987).
5. Y. LE PAGE, T. SIEGRIST, S. A. SUNSHINE, L. F. SCHNEEMEYER, D. W. MURPHY, S. M. ZAHURAK, J. V. WASZCZAK, W. R. McKINNON, J. M. TARASCON, G. W. HULL, AND L. H. GREENE, *Phys. Rev. B* **36**(7), 3617 (1987).
6. P. H. HOR, R. L. MENG, Y. Q. WANG, L. GAO, Z. J. HUANG, J. BECHTOLD, K. FORSTER, AND C. W. CHU, *Phys. Rev. Lett.* **58**(18), 1891 (1987).
7. A. FREIMUTH, S. BLUMENRODER, G. JACKEL, H. KIERSPEL, J. LANGEN, G. BUTH, A. NOWACK, H. SCHMIDT, W. SCHLABITZ, E. ZIRNGIEBL, AND E. MORSEN, *Z. Phys.* **68**, 433 (1987).
8. N. YAMAMOTO, Y. HIROTSU, Y. MURATA, S. NAGAKURA, AND M. TAKATA, *J. Electron Microsc.* **36**(4), 256 (1987).
9. S. TAKEDA AND S. HIKAMI, *Japan. J. Appl. Phys.* **26**, L848 (1987).
10. S. HIKAMI, S. KAGOSHIMA, S. KOMIYA, T. HIRAI, H. MINAMI, AND T. MATSUMI, *Japan. J. Appl. Phys.* **26**, L347 (1987).
11. Z. FISK, J. D. THOMPSON, E. ZIRINGIEBL, J. L. SMITH, AND S. W. CHEONG, *Solid State Commun.* **62**, 743 (1987).
12. F. HULLIGER AND H. R. OTT, *Z. Phys. B* **67**, 291 (1987).
13. J. HAUCK, *Solid State Commun.* **64**, 1217 (1987).
14. L. F. SCHNEEMEYER, J. V. WASZCZAK, S. M. ZAHORAK, R. B. VAN DOVER, AND T. SIEGRIST, *Mater. Res. Bull.* **22**, 1467 (1987).
15. A. K. RAYCHAVDHURI, K. SREEDHAR, K. P. RAJEEV, R. A. MOHAN RAN, P. GANGULY, AND C. N. R. RAO, *Philos. Mag. Lett.* **56**, 29 (1987).
16. R. A. MOHANRAN, N. Y. VANANTHACHARYA, P. GANGULY, AND C. N. R. RAO, *J. Solid State Chem.* **69**, 186 (1987).
17. M. A. BENO, L. SODERHOLM, D. W. CAPONE, J. D. JORGENSEN, I. K. SCHULLER, C. U. SEGRE, K. ZHANG, AND J. D. GRACE, *Appl. Phys. Lett.* **51**, 57 (1987).
18. R. J. CAVA, B. BATLOGG, R. B. VAN DOVER, D. W. MURPHY, S. SUNSHINE, T. SIEGRIST, J. P. REMEIKA, E. A. RIETMAN, S. ZAHURAK, AND G. P. ESPINOSA, *Phys. Rev. Lett.* **58**, 1676 (1987).
19. R. M. HAZEN, L. W. FINGER, R. J. ANGEL, C. T. PREWITT, N. L. ROSS, H. K. MAO, C. G. HADIDIACOS, P. H. HOR, R. L. MENG, AND C. W. CHU, *Phys. Rev. B* **35**, 7238 (1987).
20. F. ISUMI, H. ASANO, AND T. ISHIGAKI, *Japan. J. Appl. Phys.* **26**, L617 (1987).
21. L. D. MARKS, J. P. ZHANG, S. J. HWU, AND K. R. POEPPELMEIER, *J. Solid State Chem.* **69**, 189 (1987).
22. Y. SYONO, M. KIKUCHI, K. OH-ISHI, K. HIRAGA, H. ARAI, Y. MATSUI, N. KOBAYASHI, T. SASAOKA, AND Y. MUTO, *Japan. J. Appl. Phys.* **26**, 1498 (1987).
23. Y. HIROTSU, Y. NAKAMURA, Y. MURATA, S. NAGAKURA, T. NISHIHARA, AND M. TAKATA, *Japan. J. Appl. Phys.* **26**, L1168 (1987).
24. G. VAN TENDELOO, H. W. ZANDBERGEN, AND S. AMELINCKS, *Solid State Commun.* **63**, 389 (1987).
25. G. VAN TENDELOO, H. W. ZANDBERGEN, AND S. AMELINCKS, *Solid State Commun.* **63**, 603 (1987).
26. Y. MATSUI, E. TAKAYAMA-MUROMACHI, A. ONO, S. HORIUCHI, AND K. KATO, *Japan. J. Appl. Phys.* **26**, L777 (1987).
27. F. M. MUELLER, S. P. CHEN, M. L. PRUEITT, J. F. SMITH, J. L. SMITH, AND D. WOHLLEBEN, *Phys. Rev. B* **37**, 5837 (1988).
28. Y. MATSUI, Y. KITAMI, M. YOKOYAMA, N. IYI, E. TAKAYAMA-MUROMACHI, AND S. TAKEKAWA, *J. Electron Microsc.* **36**, 246 (1987).
29. Y. KITANO, I. MUKOUDA, Y. KOMURA, H. FUJII, AND T. OKAMOTO, *J. Electron Microsc.* **36**, 241 (1987).
30. D. J. LI, H. SHIBAHARA, J. P. ZHANG, AND L. D. MARKS, *Mater. Res. Soc. Symp. Proc.* **99**, 557 (1987).
31. L. D. MARKS, D. J. LI, H. SHIBAHARA, AND J. P. ZHANG, *J. Electron Microsc. Tech.* **8**, 297 (1988).
32. H. W. ZANDGERGEN, G. VAN TENDELOO, T. OKABE, AND S. AMELINCKS, *Phys. Status Solidi A* **103**, 45 (1987).
33. A. OURMAZED, J. A. RENTSHLER, J. C. H. SPENCE, M. O'KEEFFE, R. J. GRAHAM, D. W. JOHNSON, JR., AND W. W. RHODES, *Nature (London)* **327**, 308 (1987).
34. E. A. HEWAT, M. DUPUY, A. BOURRET, J. J. CAPPONIU, AND M. MAREZIO, *Nature (London)* **327**, 400 (1987).
35. D. J. LI, H. SHIBAHARA, J. P. ZHANG, AND L. D. MARKS, *Phys. C* **156**, 201 (1988).

36. T. KOGURE, R. KONTRA, G. J. YUREK, AND J. B. VANDER SANDE, *Phys. C* **156,** 45 (1988).

37. A. F. MARSHALL, R. W. BARTON, K. CHAR, A. KAPITUINIK, B. OH, AND R. H. HAMMOND, "Material Research Society, Spring Meeting," p. 197 (1988).

38. T. KOGURE, R. KONTRA, AND J. B. VANDER SANDE, *Phys. C* **156,** 35 (1988).

39. P. MARSH, R. M. FLEMING, M. L. MANDICH, A. M. SANTOLO, J. KWO, M. HONG, L. J. MARTINEZ-MIRANDA, *Nature (London)* **334,** 141, (1988).